

Supporting Online Materials

A Phenylalanine Clamp Catalyzes Protein Translocation Through The Anthrax

Toxin Pore

Bryan A. Krantz, Roman A. Melnyk, Sen Zhang, Stephen J. Juris, D. Borden Lacy,

Zhengyan Wu, Alan Finkelstein, R. John Collier

Material and Methods

Proteins. Recombinant LF_N (residues 1-263 of LF) was expressed, purified, and freed of its six-His tag by bovine α -thrombin treatment, as previously described (S1). Recombinant WT PA (and all mutants described herein) were expressed in the periplasm of *E. coli* BL21(DE3), purified, and converted to prepore heptamer as described (S2, S3).

EPR. F427C PA was labeled with a paramagnetic spin label, (1-Oxyl-2,2,5,5-tetramethyl-3-pyrroline-3-methyl) methanethiosulfonate (MTSL, Toronto Research Chemicals) (S4). Homogeneously labeled PA's were converted to prepore heptamer and concentrated to 10 mg/ml in 20 mM Tris-Cl, 200 mM NaCl, pH 8.5. Labeled prepore samples were converted to the SDS-resistant pore form by lowering the pH to 6. EPR spectra were acquired in a Bruker EMX spectrometer, where 30 scans were averaged and normalized for peak area.

Electrophysiology. Planar lipid bilayers were painted (S5) onto a 200 μ M aperture of a 1 mL delrin cup, using 3% 1,2-diphytanoyl-*sn*-glycerol-3-phosphocholine (DPhPC) in *n*-decane. Cis (side to which PA₆₃ prepore heptamer and LF_N are added) and trans compartments were generally bathed in symmetric universal bilayer buffer (UBB):

100 mM KCl, 1 mM EDTA and 10 mM each of potassium oxalate, phosphate, and MES, pH 5.5. Macroscopic current responses to steps in voltage were recorded as previously described (*S1*). $\Delta\psi$, the membrane potential, is defined as $\Delta\psi = \psi_{\text{cis}} - \psi_{\text{trans}}$, where $\psi_{\text{trans}} \equiv 0$ mV. Single-channel measurements were obtained using DphPC/decane films formed on a 50 μM aperture in a polystyrene cup (*S6*). Unitary conductance measurements were carried out at $\Delta\psi = +20$ mV (except for F427W, which was +100 mV) in symmetric 100 mM KCl, 1 mM EDTA, 25 mM potassium succinate, pH 5.5.

PA₆₃ channel formation and LF_N conductance block. Once a membrane was formed, PA₆₃ prepore heptamer (25 pM) was added to the cis compartment, which was held at a $\Delta\psi$ of +1 to +20 mV with respect to the trans compartment. LF_N was added to the cis compartment after PA₆₃ channel formation stabilized. The progress of LF_N binding to PA₆₃ channels was monitored by the continuous fall in conductance.

Voltage-jump translocation experiments. After LF_N conductance block of PA₆₃ channels was complete, excess LF_N was removed from the cis compartment with perfusion, using Microlab 500 dual syringe titrator (Hamilton, Reno, NV) configured in a push-pull arrangement. The cis compartment was perfused with 10 ml of UBB at a flow rate of 2 ml/min and at $\Delta\psi$ ranging from +1 to +20 mV. Translocation of LF_N was initiated by jumping the $\Delta\psi$ to a higher positive voltage.

Substituted cysteine accessibility modification (SCAM). MTS-ET ([2-(trimethylammonium) ethyl]methanethiosulfonate, Toronto Research Chemicals) modification of site-directed cysteine mutants of the PA₆₃ pore were analyzed in macroscopic planar lipid bilayer conductance studies as previously (*S7*). After the

trypsin-nicked PA₈₃ Cys mutant was added to the cis compartment, the conductance rose to a steady-state level (g). Following MTS-ET addition to the trans side at a final concentration of 20 $\mu\text{g/ml}$, the conductance fell to a new steady-state level (g_{block}). The fraction of conductance blocked by MTS-ET modification, f_{block} , is derived from $f_{block} = 1 - g_{block} / g$.

Conductance blocking studies. QAP and related model compounds were purchased from Sigma-Aldrich. (Table S1 lists catalog numbers.) Equilibrium QAP channel-blocking studies were performed as described (S8) by adding stock solutions symmetrically at +20 mV. Equilibrium dissociation constants, K_D , were obtained from fits to the normalized conductance (g_{norm}) profiles by using a single ligand (L) binding site model, $g_{norm} = 1 - 1 / (1 + K_D/[L])$; some F427 mutants required a model with two independent binding sites, $g_{norm} = 1 - A_1 / (1 + K_{D1}/[L]) - A_2 / (1 + K_{D2}/[L])$, where the second amplitude, A_2 , was minor, $\sim 10\%$.

Solvation energy analysis. Three-dimensional structural models of compounds were generated in CHEMOFFICE 2005 (Cambridgesoft). For the solvation term, $\Delta G_s = \sum \sigma_i A_i$, where solvent accessible surface areas, A_i , of each atom, i , were calculated by GETAREA 1.1 (S9) using a 1.4 Å probe radius and atomic solvation parameter σ -values (in $\text{kcal mol}^{-1} \text{Å}^{-2}$) from Wesson and Eisenberg for all atom types (S10), except halogen and phosphonium atoms (S11). ΔG_{aro} is an empirically based term (i.e. $\Delta G_{aro} = \alpha n$) determined using linear least squares analysis of the correlation of the experimentally determined binding energies and the expected energy from ΔG_s alone, where α is in units of $\text{kcal mol}^{-1} \text{aromatic ring}^{-1}$, and n is the number of aromatic rings per compound. The

linear least squares analysis also calculated an offset constant, c , such that the expected energy (ΔG_{theo}) was defined by $\Delta G_{theo} = \Delta G_s + \Delta G_{aro} + c$. Images of compounds used in Fig. 3 were rendered using SWISS-PDBVIEWER 3.7 and POV-RAY 3.1

Cellular LF_N-DTA translocation assay. LF_N-DTA translocation assays of F427 PA mutants were performed as described (S12). PA-dependent translocation of LF_N-DTA is reported by the DTA domain, which is the enzymatic domain of diphtheria toxin that inhibits cellular protein synthesis. Translocation of the DTA domain into the cell is measured by ³H-leucine incorporation into total cellular protein following treatment with varying concentrations of PA and a fixed LF_N-DTA concentration (1 nM).

Supporting Text

Is the PA₆₃ pore formed in solution comparable to that formed in the membrane? Without the crystallographic structure of the PA₆₃ pore, it is not certain that the pore's β -barrel formed in solution is identical to that formed in membranes. However, circumstantial evidence for this is strong. The SDS-dissociable prepore converts to an SDS-resistant pore in response to low pH on cells and in solution (*S13*). PA N306C (a Cys site in the transmembrane region of the β -barrel), when labeled with pyrene-maleimide, formed a strong excimer upon conversion to the pore in solution under acidic pH conditions (*S2*). Thus the seven β -hairpins from each of the PA₆₃ monomers cluster in the pore that forms in solution. Single channel unitary conductance data (Fig. 1F) were presented in this report to support the view that the pore formed in membranes has narrowly apposed F427 sites, thereby corroborating the EPR measurement of the pore formed in solution (Fig. 1E). These new F427 data argue further that the pore formed in solution is similar to that formed in membranes.

	411	427	438
Iota	Y	Q	Q
Sb	Y	Q	Q
CdtB	Y	Q	Q
C2	Y	Q	Q
Isp1a	Y	D	Q
Isp1b	Y	D	Q
Vip1AC	Y	D	Q
PA_atx	Y	D	Q
PA_cer	Y	D	Q

Figure S1. Sequence alignment of PA and homologous toxins at the ϕ -clamp site.

CLUSTALW (S14) was used to align the protein sequence adjacent to F427 in PA_atx from *Bacillus anthracis* (residues 411 to 438 numbered according to PA_atx, pdb 1ACC) with homologous toxins: PA_cer (accession no. ZP_00236306) from *Bacillus cereus* G9241, Iota toxin component Ib (CAA51960) from *Clostridium perfringens*, Sb component (CAA66612) from *Clostridium spiroforme*, CdtB (AAF81761) from *Clostridium difficile*, C2 toxin from *Clostridium botulinum* (BAA32537), Isp1a (CAI40767) and Isp1b (CAI43278) from *Brevibacillus laterosporus*, and Vip1Ac (AAO86514) from *Bacillus thuringiensis*. Color shading indicates dominant-negative mutations (S15, S16) either in pore formation, Y411, N422, and D425 (cyan), or in protein translocation, F427 (red).

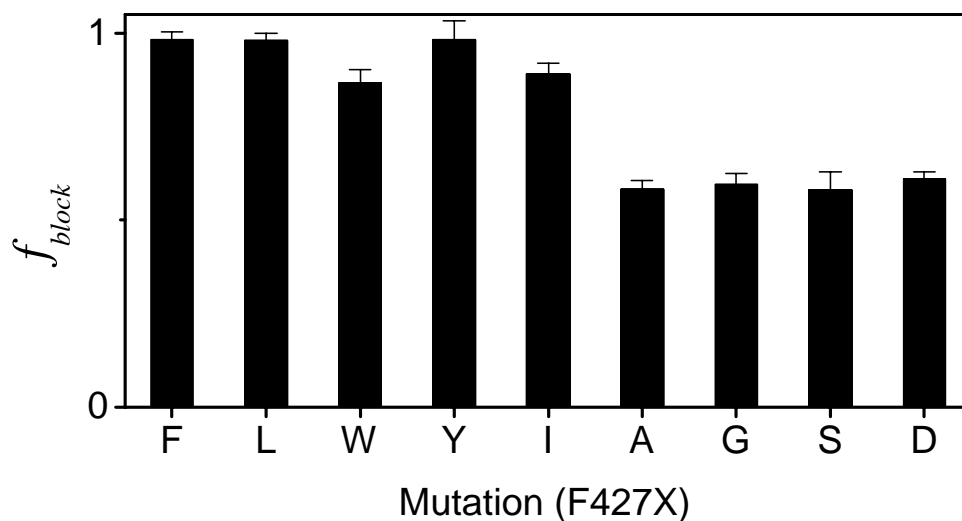


Figure S2. Effect of F427 ϕ -clamp site substitutions on LF_N conductance block. A comparison of the LF_N conductance block of WT and F427X substituted variants of PA_{63} channels under macroscopic conditions ($\Delta\psi = +20$ mV, pH 5.5) when a constant concentration of LF_N (20 nM) was added only to the cis compartment. The bars indicate the fraction of the PA_{63} channel conductance blocked (f_{block}) after LF_N binding achieved equilibrium. Error bars are standard errors (σ_{SE}) that were estimated from at least two measurements for each mutant. Even though the partial block observed for A, G, S and D substituted channels may appear insubstantial, the LF_N concentration dependence presented in Fig. 2C shows that F427A channels are, in fact, ~ 100 -fold less sensitive to LF_N than WT channels.

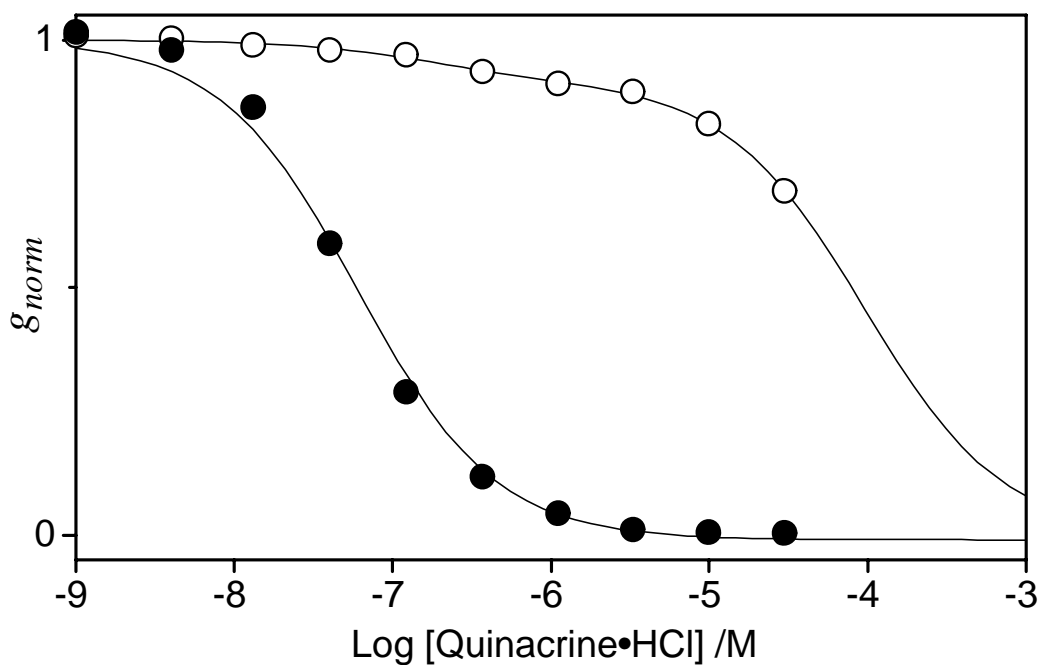


Figure S3. The F427 ϕ -clamp site is the 4-aminoquinolone drug-binding site. For conductance-blocking studies, PA₆₃ channels formed in planar lipid bilayers were blocked by adding quinacrine·HCl symmetrically to the cis and trans compartments ($\Delta\psi = +20$ mV, pH 5.5). g_{norm} was recorded after blocking reached equilibrium. For quinacrine block, a single binding site model was applied to WT PA₆₃ channels (●), $K_D = 60(\pm 5)$ nM, but a two-binding site model was required for F427A PA₆₃ channels (○), such that the major amplitude (91%) had a K_D of $96(\pm 3)$ μ M and the minor amplitude (9%) had a K_D of $0.2(\pm 0.03)$ μ M.

Table S1. PA₆₃ conductance block by model QAP and other cationic compounds.

Cationic Species	Catalog no.	K_D	ΔG_{exp} (kcal mol ⁻¹)	ΔG_s (kcal mol ⁻¹)	n	ΔG_{aro} (kcal mol ⁻¹)	ΔG_{theo} (kcal mol ⁻¹)
(2-acetylamino-2,2-bis-ethoxycarbonyl-ethyl)-trimethyl-ammonium	R410217	1.0(±0.1) mM	4	1.7	0	0	2.5
Adamantan-1-yl-diethyl-methyl-ammonium	S40380	6.6(±0.3) μM	6.9	4.7	0	0	5.5
Allyl-benzyl-diethyl-ammonium	R225614	18(±1) μM	6.3	5.1	1	0.7	6.6
3-benzyl-1,2-dimethyl-3H-benzimidazol-1-ium	R770442	6.5(±0.3) μM	6.9	5.3	2	1.5	7.5
Benzyltributylammonium	13954	2.5(±0.2) μM	7.5	6.9	1	0.7	8.3
Benzyltriethylammonium	147125	21(±3) μM	6.2	4.8	1	0.7	6.3
Benzyltrimethylammonium	147117	65(±5) μM	5.6	4.1	1	0.7	5.6
Benzyltriphenylphosphonium	430056	110(±30) nM	9.3	6.8	4	2.9	10.5
(2-(2,2-bis-ethoxycarbonyl-vinylamino)-ethyl)-trimethyl-ammonium	R417831	540(±30) μM	4.4	0.9	0	0	1.7
2-butoxy-4-ho-6-ph-octahydro-pyrano(3,2-b)pyran-3-yl-trimethyl-ammonium	S469661	49(±4) μM	5.8	4.3	1	0.7	5.8
Butyltriphenylphosphonium	B102806	88(±5) nM	9.4	6.6	3	2.2	9.6
Chloroquine	C6628	510(±30) nM	8.4	4	2	1.5	6.2
Denatonium benzoate	348538	81(±7) μM	5.5	5	2	1.5	7.2
1,3-dibenzyl-2-methyl-3H-benzimidazol-1-ium	R770426	6.4(±0.4) μM	6.9	6.6	3	2.2	9.5
1,1-Dimethyl-4-phenylpiperazinium	D5891	37(±2) μM	5.9	4.8	1	0.7	6.2
Dimethyldiphenylphosphonium	346594	5.9(±0.2) μM	7	4.7	2	1.5	6.9
(1,2-diphenyl-propyl)-trimethyl-ammonium	S325554 S325570	2.9(±0.2) μM 6(±0.4) μM	7.4 7	5.6	2	1.5	7.8
Fluphenazine	F4765	1.3(±0.2) μM	7.9	3	3	2.2	5.9
Isoamyltriphenylphosphonium	347779	35(±6) nM	10	6.9	3	2.2	9.8
(7-isopropyl-1,4a-di-me-octahydro-phenanthren-1-ylmethyl)-trimethyl-ammonium	S303550	4.1(±0.3) μM	7.2	6.9	1	0.7	8.4
Methyl viologen	856177	78(±13) μM	5.5	4.8	2	1.5	7
Methyltriphenylphosphonium	468002	370(±60) nM	8.6	5.5	3	2.2	8.4
Quinacrine	Q3251	60(±5) nM	9.6	5.2	3	2.2	8.1
Tetrabutylammonium	86857	7.3(±0.2) μM	6.9	6.8	0	0	7.5
Tetrabutylphosphonium	189138	1.4(±0.1) μM	7.8	6.8	0	0	7.6
Tetraethylammonium	86610	224 μM	4.9	4	0	0	4.7
Tetrahexylammonium	87302	3.8(±0.3) μM	7.2	9.6	0	0	10.3
Tetramethylammonium	87710	1.6 mM	3.7	3	0	0	3.7

Cationic Species	Catalog no.	K_D	ΔG_{exp} (kcal mol ⁻¹)	ΔG_s (kcal mol ⁻¹)	n	ΔG_{aro} (kcal mol ⁻¹)	ΔG_{theo} (kcal mol ⁻¹)
Tetrapentylammonium	87997	2 μ M	7.6	8.1	0	0	8.9
Tetraphenylphosphonium	218782	46(\pm 2) nM	9.8	6.2	4	2.9	9.9
Tetrapropylammonium	88105	350(\pm 10) μ M	4.6	4.9	0	0	5.6
Trimethyl-(3-oxo-2,5-diphenyl-pent-4-enyl)-ammonium	R254967	3.2(\pm 0.2) μ M	7.3	4.4	2	1.5	6.6
1,2,3-trimethyl-3H-benzimidazol-1-ium	S30032	1.6(\pm 0.4) mM	3.7	4.2	1	0.7	5.7
Trimethylphenylammonium	135321	70(\pm 20) μ M	5.5	3.8	1	0.7	5.3
Trimethylphenylphosphonium	488151	12(\pm 2) μ M	6.6	3.9	1	0.7	5.3

Legend for Table S1. Only the cation from each compound is listed. Counter-ions were generally bromide or chloride. Catalog nos. are from Sigma-Aldrich. K_D : binding equilibrium constant estimated generally for a single-site binding model, where errors (σ_{SD}) are estimated from the non-linear least squares fit of the binding curve; in some cases, a second binding site was required to fit the data. In those cases, the second site had a minor amplitude of \sim 10%, and only the major amplitude K_D is reported. ΔG_{exp} : experimental binding free energy at the blocking site calculated by $\Delta G_{exp} = RT \ln K_D$. ΔG_s : Wesson and Eisenberg solvation energy ($S10$) calculated from the solvent accessible surface area. n : the number of aromatic rings contained in each compound. ΔG_{aro} : aromatic enhancement binding energy given as $\Delta G_{aro} = \alpha n$, where α is 0.7(\pm 0.3) kcal mol⁻¹ aromatic ring⁻¹. ΔG_{theo} : total expected energy calculated by $\Delta G_{theo} = \Delta G_s + \Delta G_{aro} + c$, where the calculated offset constant, c , was 0.8(\pm 0.4) kcal mol⁻¹. (See also Fig. 3F.) The two observations made for (1,2-diphenyl-propyl)-trimethyl-ammonium are for different preparations of the compound. K_D values for tetraethylammonium, tetramethylammonium, and tetrapentylammonium were taken from a previous study ($S8$).

Table S2. Cys substitution effects on PA₆₃ channel-forming activity.

Relative channel-forming activity (% of WT)	Residue
<0.01	363, 364, 375, 379, 380, 382, 391, 393, 394, 397, 399, 411, 420, 422, 425, 432, 454
0.01 - 0.1	376, 400, 426, 431, 435
0.1 - 10	377, 378, 381, 388, 390, 408, 419, 421, 451, 465, 466, 480
>10	361, 369, 374, 383, 384, 385, 386, 392, 395, 396, 398, 401, 402, 409, 413, 414, 415, 416, 423, 424, 427, 428, 429, 430, 433, 434, 436, 437, 439, 440, 449, 453, 455, 456, 458, 459, 460, 461, 463, 464, 467, 469, 470, 471, 472, 473, 474, 476, 478, 479, 482

Relative channel-forming activity in DPhPC/decane bilayers. The activity percentage is determined from the macroscopic conductance generated per nanogram of each Cys-substituted mutant at the indicated residues versus WT PA₆₃.

References and Notes

- S1. S. Zhang, A. Finkelstein, R. J. Collier, *Proc. Natl. Acad. Sci. U.S.A.* **101**, 16756 (2004).
- S2. C. J. Miller, J. L. Elliott, R. J. Collier, *Biochemistry* **38**, 10432 (1999).
- S3. D. J. Wigelsworth *et al.*, *J. Biol. Chem.* **279**, 23349 (2004).
- S4. K. J. Oh, C. Altenbach, R. J. Collier, W. L. Hubbell, *Methods Mol. Biol.* **145**, 147 (2000).
- S5. P. Mueller, D. O. Rudin, H. T. Tien, W. C. Westcott, *J. Phys. Chem.* **67**, 534 (1963).
- S6. R. O. Blaustein, E. J. Lea, A. Finkelstein, *J. Gen. Physiol.* **96**, 921 (1990).
- S7. E. L. Benson, P. D. Huynh, A. Finkelstein, R. J. Collier, *Biochemistry* **37**, 3941 (1998).
- S8. R. O. Blaustein, A. Finkelstein, *J. Gen. Physiol.* **96**, 905 (1990).
- S9. R. Fraczekiewicz, W. Braun, *J. Comp. Chem.* **19**, 319 (1998).
- S10. L. Wesson, D. Eisenberg, *Protein Sci.* **1**, 227 (1992).
- S11. J. Wang, W. Wang, S. Huo, M. Lee, P. A. Kollman, *J. Phys. Chem. B* **105**, 5055 (2001).
- S12. B. R. Sellman, S. Nassi, R. J. Collier, *J. Biol. Chem.* **276**, 8371 (2001).
- S13. J. C. Milne, D. Furlong, P. C. Hanna, J. S. Wall, R. J. Collier, *J. Biol. Chem.* **269**, 20607 (1994).
- S14. J. D. Thompson, D. G. Higgins, T. J. Gibson, *Nucleic Acids Res.* **22**, 4673 (1994).
- S15. B. R. Sellman, M. Mourez, R. J. Collier, *Science* **292**, 695 (2001).

S16. M. Mourez *et al.*, *Proc. Natl. Acad. Sci. U.S.A.* (2003).